

University of Nebraska - Lincoln

DigitalCommons@University of Nebraska - Lincoln

Dissertations & Theses in Earth and Atmospheric
Sciences

Earth and Atmospheric Sciences, Department of


Winter 12-3-2018

CALCAREOUS NANNOFOSSIL BIOSTRATIGRAPHY AND PALEOECOLOGY OF THE FORT HAYS LIMESTONE OF WESTERN KANSAS, WESTERN INTERIOR BASIN (WIB)

Bryan Hermosillo

University of Nebraska - Lincoln, bhermos7@gmail.com

Follow this and additional works at: <http://digitalcommons.unl.edu/geoscidiss>

 Part of the [Earth Sciences Commons](#), and the [Oceanography and Atmospheric Sciences and Meteorology Commons](#)

Hermosillo, Bryan, "CALCAREOUS NANNOFOSSIL BIOSTRATIGRAPHY AND PALEOECOLOGY OF THE FORT HAYS LIMESTONE OF WESTERN KANSAS, WESTERN INTERIOR BASIN (WIB)" (2018). *Dissertations & Theses in Earth and Atmospheric Sciences*. 112.

<http://digitalcommons.unl.edu/geoscidiss/112>

This Article is brought to you for free and open access by the Earth and Atmospheric Sciences, Department of at DigitalCommons@University of Nebraska - Lincoln. It has been accepted for inclusion in Dissertations & Theses in Earth and Atmospheric Sciences by an authorized administrator of DigitalCommons@University of Nebraska - Lincoln.

**CALCAREOUS NANNOFOSSIL BIOSTRATIGRAPHY AND PALEOECOLOGY
OF THE FORT HAYS LIMESTONE OF WESTERN KANSAS, WESTERN
INTERIOR BASIN (WIB)**

by

Bryan Hermosillo

A THESIS

Presented to the Faculty of
The Graduate College at the University of Nebraska
In Partial Fulfillment of Requirements
For the Degree of Master of Science

Major: Earth and Atmospheric Sciences

Under the Supervision of Professor David K Watkins

Lincoln, Nebraska

December 2018

**CALCAREOUS NANNOFOSSIL BIOSTRATIGRAPHY AND PALEOECOLOGY
OF THE FORT HAYS LIMESTONE OF WESTERN KANSAS, WESTERN
INTERIOR BASIN (WIB)**

Bryan Hermosillo, M.S.

University of Nebraska, 2018

Advisor: David K. Watkins

Investigations of Upper Cretaceous hemi-pelagic sediments from the Western Interior Basin suggest that high surface water fertility caused increased production of biogenic carbonate, resulting in the deposition of limestone. We examined calcareous nannofossils from the Turonian/Coniacian Fort Hays Member of the Niobrara Formation to evaluate the correlation between nannofossil surface water fertility proxies and associated lithology. Our paleoecology results indicate that oligotrophic surface water conditions were present during limestone deposition. This stands at odds with existing depositional models for the Western Interior Seaway (WIS). Paleoecological data within the interbedded marls was artificially skewed due to the prevalence of etching caused by diagenetic overprinting. This occurred during burial and caused the remobilization of calcite from marls into the adjacent limestones, resulting in $\delta^{18}\text{O}$ excursions within the marls. The first occurrence datum FAD of the species *Micula cubiformis* is proposed as a proximal nannofossil substitute for the FAD of the inoceramid biomarker *Cremonoceramid deformis erectus* throughout the Western Interior Basin (WIB).

TABLE OF CONTENTS:	PAGE:
TITLE PAGE	i
ABSTRACT	ii
TABLE OF CONTENTS	iii
LIST OF FIGURES	iv
LIST OF TABLES	v
INTRODUCTION	1
MATERIALS AND METHODS	4
RESULTS	7
DISCUSSION	9
CONCLUSION	18
REFERENCES	27
TAXONOMIC PLATE 1	30
TAXONOMIC PLATE 2	31

LIST OF FIGURES:	PAGE:
FIGURE 1: LOCALITY MAP	21
FIGURE 2: STRATIGRAPHIC COLUMN	22
FIGURE 3: PRINCIPLE COMPONENT (PCA) 1 PLOT	23
FIGURE 4: PCA1 1 VS PCA2 PLOT	23

LIST OF TABLES:	PAGE:
TABLE 1: PRESERVATION CLASSIFICATION	24
TABLE 2: NANNOFOSSIL TAXONOMY	24
TABLE 3: LINEAR CORRELATIONS FOR FIGURE 2	24
TABLE 4: PALEOECOLOGICAL RESULTS	25
TABLE 5: GEOCHEMICAL RESULTS	25
TABLE 6: DISSOLUTION RESISTANT SPECIES	26
TABLE 7: DISSOLUTION PRONE SPECIES	26

1. Introduction

Statement of Problem

Quantitative analyses of calcareous nannofossil assemblages serve as cogent surface water fertility proxies. Research on Upper Cretaceous nannofossil assemblages within the Western Interior Basin (WIB) have focused primarily on episodes of elevated primary productivity (Watkins, 1989; Bowman and Bralower, 2005; Brace and Watkins, 2014). The paucity of data on low fertility assemblages has resulted in a limited understanding of how biogenic sediment accumulation rates affect lithology within hemipelagic depositional environments (Hattin, 1982; Lafierrie et al., 1992). A decimeter-scale biostratigraphic and paleoecological study of calcareous nannofossil assemblages was conducted from samples within the Fort Hays Member of the Niobrara Formation, in order to delineate the effects of surface water fertility on Upper Cretaceous carbonate sedimentation within the WIB.

The paucity of macrofossil biostratigraphic marker species, coupled with unconformities and diachronous member contacts, complicates the chronostratigraphy of the Fort Hays Member. The use of absolute biomarkers in conjunction with radiometric dates allows the temporal constraint on large intervals of Fort Hays Member sections (Sageman et al., 2014). These markers are not present throughout all Fort Hays sections; however, the continuity of interbedded limestones and marls/shales with time parallel bentonite seams, allows for correlations across isochronous sections (Laferrriere, 1992). The base of the Coniacian is estimated by correlating time parallel bentonite seams and limestone/shale couplets containing the inoceramid *Cremnoceramus deformis erectus* first appearance datum (FAD).

2. Background

2.1 Regional setting

Mesozoic crustal loading onset by the subduction of the Farallon Plate below the western North American craton created a retroarc foreland basin (Kauffman, 1977; Kauffman and Caldwell, 1993). An epeiric seaway flooded the resultant basin and was subsequently filled by hemi-pelagic sediments eroded off the Sevier Highlands to the west (Figure 1; Kauffman, 1977). Infill was deposited during 3-4 transgressive-regressive sequences throughout the Cretaceous, forming the Greenhorn and the Niobrara Cyclothem. The WIB connected the Arctic and the Gulf Coast during maximum transgressions from north to south, and east to west from Iowa to Central Utah (Figure 1; Kauffman, 1977; Kauffman and Caldwell, 1993).

2.2 Lithostratigraphy

The Niobrara Formation was first documented from outcrops near the confluence of the Niobrara and Missouri rivers in northeast Nebraska (Meek and Hayden, 1861). The transgressive-regressive cycles within the WIB resulted in unconformities between member contacts. The Fort Hays Member unconformably overlies the regressive sequence of the Codell Sandstone and Juana Lopez Calcarenite Members of the Carlile Shale across the WIB (Hattin, 1975; Kita and Watkins, 2014). The Niobrara Formation was divided into the lower Fort Hays Member and the overlying Smoky Hill Shale Member by Logan (1897). The Fort Hays section in Western Kansas (Locality 1, Trego County) consists of relatively thick (15.3-110 cm) cliff forming limestone units, interbedded with marl/shale (2.5-42.7 cm) and bentonite (0.9-3.1 cm) seams (Figure 3).

Recesses form between limestone ledges due to the propensity of marl, shale, and bentonite to erode in outcrop. The overlying Smokey Hill Member contains a higher proportion of relatively thick marl units, resulting in exposed sections receding at member contacts. This erosional disparity forms a characteristic bench across western Kansas, eastern Colorado, northern New Mexico, and Nebraska (Hattin, 1982). Pratt (1981) noticed that clastic-rich lithologies were thicker and more prolific in localities proximal to the detritus shed off the Sevier Highlands to the west. Conversely, marl and limestone beds became thicker and more prevalent near eastern cratonic lowlands (Figure 1), where biogenic carbonate was the primary sedimentary constituent (Hattin 1982; Laferriere, 1992).

Oscillations between limestones and interbedded marls/shales occur in distinct patterns across the basin (Hattin, 1982; Laferriere, 1992). Gilbert (1895) was the first to associate this rhythmicity throughout the Niobrara Formation with Milankovitch cyclicity, consisting of five-fold bedding cycles of limestone and shale/marl couplets. Bedding cyclicity was interpreted as precessional cycles, each lasting approximately 20 kyr (Gilbert, 1895; Eicher and Diner, 1985). Three contrasting depositional models have been proposed to explain the origin of these orbitally-forced hemipelagic cycles. The “dilution model” of Pratt (1981) postulated that periodic variances of terrigenous detrital influx diluted an assumed constant background biogenic carbonate production and sedimentation (Pratt, 1981). Conversely, the “productivity model” proposed that varying biogenic carbonate production rates diluted the assumed rate of constant terrigenous detrital input rate of Eicher and Diner (1985). A ‘diagenetic model’ involves the remobilization of carbonate across clay-rich lithologies to clay-poor lithologies

(Laferriere, 1992). The preferred models vary from west to east across the WIB, depending on the primary source of sediment at a given point within the basin, and the relative influence of burial diagenesis. The dilution model has been advocated for localities proximal to the Sevier Highlands (Figure 1) by Scott and Cobban (1964) and Bralower and Bergen (1998). In contrast, studies (Boesiger, 2005; Kita and Watkins, 2014) that documented comparably higher biogenic carbonate production relative to clastic input near the eastern lowlands support the productivity model.

3. Materials and Methods

3.1 Calcareous Nannofossils

Samples were collected at 10 cm intervals through 21.3 m of the Fort Hays Member of the Niobrara Formation from outcrop exposures within Trego County, Kansas (Figure 1). Hattin, (1982) referred to this exposure as Locality 1 across western Kansas sections of the Niobrara Formation. Seventy-four samples from this collection were prepared into smear slides through the double slurry method (Watkins and Bergen, 2003) to yield reproducible data at the 99% confidence level. Calcareous nannofossil taxa were identified through the visual and optical differences observed under cross-polarized light, plane light, phase contrast, and through a one-quarter λ mica plate through an Olympus BX 51 light microscope at 1250x magnification. Photomicrographs were captured with an Olympus DP71 camera. Nannofossil percent abundance data were collected in 0.1-0.5 m intervals by counting at least 456 specimens per sample to yield percent abundance data at the 95% confidence interval (Chang, 1967). Counting was followed by a 30-minute scan of additional fields-of-view to identify rare taxa. Of the 74 samples examined, presence/absence data was gathered from 31 samples by examining one

transect (120 fields of view) across each sample in search for the FAD of marker species in decimeter increments. In total, this study compiled quantitative data from 74 samples.

Roth's (1978) preservational scheme (Table 1) by was used to qualitatively categorize relative degrees of etching and overgrowth across nannofossil assemblages (Table 1). Etching is the dissolution of delicate calcite skeletal structures, potentially resulting in complete dissolution of dissolution-prone species. Overgrowth is the precipitation of secondary calcite, which may result in the obstruction of features used for identification. Partial specimens more than 50% intact were considered complete. Fragments of *Lithraphidities carniolensis* were counted as thirds, and determined complete if both tapered ends were present. Final counts were rounded up to the nearest whole number.

3.2 Paleocological Data Analysis

The Paleontological Statistics Software (PAST) (Hammer et al., 2001) was used to statistically analyze percent abundance data to yield paleocological parameters indicative of community structure. Species richness (S) is the total number of taxa in an assemblage. Evenness (E) quantifies the relative distribution of species throughout a community (Watkins, 1986; Browning and Watkins, 2008). Shannon diversity (H) is a function of both species richness and evenness to characterize community diversity (Pielou, 1969). Principle component analysis (PCA) was used to statistically quantify and rank the amount of variation of each component. Taxa that consisted of > 3% of the total assemblage were subjected to this analysis (Figure 4). Nanofossil species below 3% of total assemblage were not considered, in order to reduce statistical noise from the prominent signal. A minimum threshold of $r > 0.70$ was used to delineate the statistical

significance of a component's contribution to variance in an assemblage. Percent abundance counts were collected from 43 of the total 74 samples selected.

Pearson's correlation coefficient was used to quantify linear correlations between two variables. The mathematical probability that an outcome occurred through random change is statistically unlikely if marginal significance values (p) are less than .05 within a sample set (n). Under these parameters, the null hypothesis is rejected and the linear relationship is deemed statistically significant.

3.3 Stable Isotopes

Raw samples selected at 10 cm intervals ($n=191$) were crushed into a fine powder before being sent for isotopic analysis at the Keck Paleoenvironmental and Environmental Stable- Isotope Laboratory at the University of Kansas. Powdered samples of bulk carbonate were flushed with ultrahigh-purity (UHP) helium for 5 minutes, injected with phosphoric acid, and left to react for 24 hours at 25°C. Samples were subsequently analyzed with the Finnigan MAT 253 isotope-ratio mass spectrometer with a ThermoFinnigan GasBench II. Results for $\delta^{13}\text{C}_{\text{carb}}$ and $\delta^{18}\text{O}$ were calculated relative to the Vienna Peedee belemnite (VPDB) standard. Analytical precision of $>0.06\text{‰}$ was attained through the use of both NBS-19 limestone and the NBS-18 carbonatite as quality-control metrics.

In preparation for $\delta^{13}\text{C}_{\text{org}}$ analysis, carbonate was removed from the samples using 0.5 molarity (M) hydrochloric acid (HCl) and subsequently freeze-dried using a Labconco Freezone 4.5 Model 77500 freeze dryer. Samples were then weighed, wrapped in 5 x 9 mm pressed tin capsules, and combusted in a Costech Instruments ECS 4010

(Elemental Combustion System). The resulting gases were continually forced via a Thermo Finnigan ConFlo III into the ThermoFinnigan MAT 253 Stable Isotope Mass Spectrometer. Results were notated relative to the VPDB standard with an analytical precision of $>0.05\%$. Weight percent total organic carbon (%TOC) values were generated as a byproduct of this process. A total of 181 samples were used for $\delta^{13}\text{C}_{\text{carb}}$, $\delta^{13}\text{C}_{\text{org}}$, and $\delta^{18}\text{O}$ results.

3.4 Carbonate content

The ratio of CaCO_3 to clastic material is used to delineate lithotypes between limestone ($>75\%$ CaCO_3) and marl ($<75\%$ CaCO_3). Percent carbonate within each sample was calculated by comparing CO_2 gas emitted between the reaction between HCl and CaCO_3 . The amount of gas released was plotted with samples throughout the Niobrara Formation to create a linear regression equation. From this linear relationship, the absolute mass of carbonate could be calculated from the CO_2 gas emitted. This was then compared to the initial mass of the sample to yield carbonate content as a percentage (Riesselman, 2000). A total of 222 carbonate content data were used in this study.

4. Results

4.1 Nannofossil Biostratigraphy

Biostratigraphic analysis yielded a total of 110 taxa. The chronological progression of recognized nannofossil marker species suggests continuous deposition throughout the entire Fort Hays Member. The FAD of three marker taxa were identified within the study section (Figure 2). The FAD of *Micula staurophora* occurs 16.8 m above the base of the Fort Hays Member and serves as a biomarker for the base of the

established CC14 Zone (Perch-Nielsen, 1985) and UC10 Zone (Burnett, 1998). The FAD of *M. adumbrata* occurs at 8.5 m, with the FAD of *M. cubiformis* occurring one meter below at 7.5 m above the base. The FAD of the inoceramid marker species *Cremnoceramus deformis erectus* defines the base of the Coniacian, is not present in our study. The acme of *Marthasterites furcatus* (>5% relative abundance) occurs exclusively within the marl (<75% carbonate) units at 14.9 m, 15.1 m, and 16.3 m (Figure 2). The co-occurrence of *Broinsonia furtiva*, *Eprolithus moratus*, *Lithastrinus septenarius*, and *Kamptnerius magnificus* at the base (.1m) of our study section implies CC13 and UC9 begin at the base of our study interval.

4.2 Paleoecology

Nannofossil taxa that constitute at least 3% of the nannofossil assemblage (Table 2) were subjected to the Principle Component Analysis. Approximately 76.8% of the variance within this assemblage is explained by the first principle component (PCA1; Figure 4). Component correlations and coefficients from PCA1 indicate that *W. barnesiae* ($r = 0.99$) correlates most negatively with *D. ignotus* ($r = -0.74$). The remaining PCA1 components did not exceed the minimum significance threshold ($r > 0.70$) to be deemed statistically significant. The four heights (14.9 m, 15.1 m, 16.3 m; Figure 2) that constitute the of species *M. furcatus* is the second principle component (PCA2) and exhibits an orthogonal relationship to *W. barnesiae* (Figure 4). These inversely associated species characterize two distinct assemblages between limestones and marls.

The fossil assemblage within the marls (<75% carbonate) is characterized by an increase of at least one standard deviation (9.47%) above the percent abundance mean (22.7%) of *W. barnesiae* (Figure 2). This species has a negative linear relationship with

%*D. ignotus*, Shannon Diversity, Evenness, species richness, percent carbonate, and correlates positively with $\delta^{13}\text{C}_{\text{carb}}$ (Figure 2; Table 3). The limestone-chalk (>75% carbonate) assemblage is characterized by an increase of at least one standard deviation (4.77) above the mean percent abundance (5.57%) of % *D. ignotus*. This species correlates positively with: Shannon diversity, evenness, species richness, percent carbonate, and correlates negatively with % *W. barnesiae*, $\delta\text{C}^{13}_{\text{carb}}$, and $\delta^{13}\text{C}_{\text{org}}$ (Figure 2; Table 3). Maxima, minima, and averages for each paleoecological parameter are summarized in Table 4.

4.3 Geochemistry

Bulk $\delta^{18}\text{O}$ carbonate correlates negatively to CaCO_3 , % *D. ignotus*, Shannon Diversity, Evenness, Richness and correlates positively with *W. barnesiae*. Bulk $\delta^{13}\text{C}_{\text{carb}}$ carbonate negatively correlates with CaCO_3 , %*D. ignotus*, Shannon Diversity, Evenness, and correlates positively with *W. barnesiae* (Figure 2; Table 3). Bulk $\delta^{18}\text{O}$ carbonate has a strong positive correlation with $\delta^{13}\text{C}_{\text{carb}}$ ($r = .292$; significant at $p < 0.01$). Both %TOC and $\delta^{13}\text{C}_{\text{org}}$ had no statistically significant correlations to any geochemical, lithologic, or paleoecologic parameter (Figure 2; Table 3). Carbonate correlates negatively with $\delta^{13}\text{C}_{\text{carb}}$ and $\delta^{18}\text{O}$ excursions within marlstones (Figure 2; Table 3). The maxima, minima, and averages of $\delta^{13}\text{C}_{\text{carb}}$, $\delta^{13}\text{C}_{\text{org}}$, $\delta^{18}\text{O}$, and %TOC are summarized in Table 5.

5.0 Discussion

5.1 Biostratigraphy

Three calcareous nannofossil bioevents were identified within the Fort Hays Member. The FAD of *M. cubiformis* is the oldest (7.5 m), followed by the FAD of *M.*

adumbrata (8.5 m), and the FAD of *M. starouphora* (16.8 m; Figure 2). This *Micula* bioevent sequence mirrors the Late Cretaceous biostratigraphic framework of Corbett, et al. (2014); however, the highest occurrence of (LAD) of *Helicolithus turonicus* differs from their results. The FAD of *H. turonicus* appears between the FAD of both *M. cubiformis* and *M. adumbrata* in Corbett, et al. (2014). In our study section, the LAD of *H. turonicus* extends to the top of the Fort Hays Member (21.3 m) and ends at the lithostratigraphic contact at the contact between the Fort Hays and Smoky Hill members. We attribute this discrepancy to different taxonomical definitions between the consistent classification of the characteristic axial central cross, relative to other species whose defining characteristic is a slightly skewed cross. Other possibilities include: major lithological change between members that result in an apparent disappearance, or temporal variances associated with the aggregated FADs and LADs of biomarker species across isochronous sections that the methodology of Corbett, et al. (2014) used to determine the order of events (Ranking and Scaling statistical method).

Laferriere (1992) correlated limestone and shale/marl couplets and time parallel bentonite seams from coeval sections across central Colorado to northern Kansas. Given these correlations, the second couplet containing the FAD of *C.d. erectus* can be traced across Pueblo, Colorado to locality 1 in S.W. Trego Co., KS. The FAD range of *C.d. erectus* occurs 5.8-7.3 m above the base of the Fort Hays section in Pueblo CO (Scott and Cobban, 1964) and coincides with the second shale-limestone couplet. Laferriere (1992) traced these strata across the WIB to Hattin's (1982) unit 10 (6.1-7.2 m) limestone bed (Figure 2), placing the Turonian-Coniacian boundary within this interval.

Corroborating evidence between microfossil and macrofossil estimates from the Cenomanian to Santonian WIB stratigraphic framework by Corbett et al. (2014) placed the FAD of *M. cubiformis* proximal to the FAD range of *C.d. erectus* throughout several coeval sections across the WIB. Our results concur with this framework, the FAD of *M. cubiformis* occurs 0.3-1.4m above the inferred *C.d. erectus* FAD range at our section (Locality 1, SW Trego Co., KS; Figure 1).

Biostratigraphic studies of the Bohemian Basin from the Czech Republic (Tethys Province) reveal that the FAD of *C.d. erectus* occurs near the base of the *M. furcatus* acme (Švábenick, and Bubík , 2014). This is inconsistent with the results of our study, where the inferred FAD of *C. d. erectus* (6.1-7.2) occurs below the acme (>5%; Švábenick, and Bubík , 2014) of *M. furcatus* (14.9-16.3 m; Figure 2). Calcareous nannofossils are sensitive indicators of surface water conditions, thus changes in ocean circulation would have direct influence on assemblage composition. Such changes may not be immediately ubiquitous, thus provincial differences in paleoecology between the Tethys and WIB may explain biostratigraphic differences of the *M. furcatus* acme.

5.2 Nannofossil Preservation

Nannofossil assemblages exceeding 40% mean values of the dissolution resistant species *W. barnesiae*, serve as a quality control metric for identifying sections that are too diagenetically altered to provide unbiased nannofossil assemblage data (Roth and Bowdler, 1981; Williams and Bralower 1995; Burns and Bralower, 1998). Paleoecological interpretations can be skewed through diagenesis by preferentially dissolving delicate taxa, while sparing more robustly calcified species. This creates a “closed sum” problem that can compromise linear relationships between variables in

poorly preserved samples (Burns and Bralower, 1998). Nannofossil assemblages within limestones contain average *W. barnesiae* (19.5%) well below the 40% threshold, indicating that nannofossil assemblages remained relatively intact after burial. Marls contain relatively higher percent abundance of *W. barnesiae* (33.1%). The elevated presence of this species within marls may be due to a combination of paleoecological shifts and differing diagenetic effects between lithologies when subjected to burial. Roth (1978) postulated that assemblages with disparate amounts of these species could have been artificially enriched as a result of dissolution. The decrease in the relative abundance of susceptible species (Table 7) suggests that these species may have been preferentially dissolved, allowing for the over representation of dissolution resistant species. The analysis of geochemical evidence provides insight into the possible mechanism(s) that lead to the disparate preservation between lithologies.

Laferriere (1992) attributed changes in preservation and isotopic excursions within the Fort Hays Member marls to burial diagenesis. Increased pressure and temperature during burial remobilized calcite between lithologies, and caused pressure solution within clay-rich marlstones. Isotopically light secondary calcite was subsequently precipitated within the adjacent limestones, resulting in the negative $\delta^{18}\text{O}$ excursions within marls. Pratt (1981) argued that this $\delta^{18}\text{O}$ geochemical trend was the result of salinity changes caused by increases in continental runoff. Through petrographic and SEM observation, Laferriere (1992) examined unaltered inoceramid material and concluded geochemistry retained a relatively unaltered signal relative the bulk carbonate matrix, which differed significantly. The presence of inoceramids indicated that conditions remained normal marine throughout both marlstone and limestone deposition. Cathodoluminescence

analysis of inoceramids indicated that the amount of pressure solution seams and isotope excursions increased with burial depth. Geochemical trends from Kansas to Colorado concur with this observation, as $\delta^{18}\text{O}$ values become more negative to the more deeply buried sediments to the west. Thus, bulk carbonate geochemistry was more of an indicator of diagenetic processes, rather than $\delta^{18}\text{O}$ flux driven by paleoenvironmental changes.

Petrographic analysis from the North Atlantic Basin (Frank et al., 1999) yielded a similar geochemical pattern and diagenetic mechanism. Burial compaction resulted in pressure solution to transfer isotopically light carbonate from carbonate-poor lithologies into adjacent carbonate-rich lithologies, causing the precipitation of secondary calcite cement. This cement depleted carbonate-rich lithologies in ^{18}O , while simultaneously preserving the original geochemical signal within the carbonate-poor interval (Frank et al., 1999). In the context of the Fort Hays Member, this fractionation process would have resulted in marls retaining their original chemical signature, while the surrounding limestones were relatively depleted in ^{18}O . Thus, the ^{18}O signal within the limestones proposed by Laferriere (1992) are actually the excursions, while the marls are representative of the original signal. This further supports the argument that bulk carbonate is not reliable proxy for salinity, thus the influx of fresh water was not sufficient to change ocean chemistry or perturb nannofossil paleoecology.

Since increases in % *W. barnesiae* and negative $\delta^{18}\text{O}$ excursions are associated with calcite remobilization and decreased nannofossil preservation, the burial diagenesis mechanism is consistent with increased etching observed within marls (E-1 to E-2; Table 1) and calcite overgrowths within limestones (O-1 to O-2; Table 1). Our observed

positive correlation between $\delta^{18}\text{O}$ and %carbonate (Figure 3; Table 3) concurs with Frank, et al., (1999) observation between positive $\delta^{18}\text{O}$ excursions (Figure 3) within limestone beds. The donation of carbonate ions into the limestones as a result of the dissolution of nanofossils, would have enriched the dissolution resistant species *W. barnesiae* (Figure 3; Table 3) within the marls. This pattern is also observed with the doubling in percent abundance of *Eprolithus* spp., *L. septanarius*, and *Q. gartnerii* (Table 6). These findings are consistent with Roth (1978), as they also documented these species as being the most dissolution resistant. Similar to %*W. barnesiae*, these species correlate negatively with %carbonate, and positively with $\delta^{18}\text{O}$ (Table 6). Unlike *M. furcatus*, the percent increases of these dissolution resistant species are insufficient to be considered an acme. Decreased preservation within marls also impeded the differentiation of species within the *Prediscospherera* genus. The obstruction or disappearance of central areas in both *P. spinosa* and *P. cretacea* increased throughout marls (Table 6).

Sharp increases of *M. furcatus* abundance above 5% (Table 6) between 14.9-16.3m (Figure 2) indicate an acme and occur exclusively within marlstones; however, the dissolution effects within marl intervals outside the acme zone were also subject to the effects of diagenesis. The characteristic angular protrusions of *M. furcatus*, common throughout the relatively well-preserved limestones, were etched into rounded stubs across all marl seams. Our acme results are temporally consistent with Švábenick, and Bubík (2014), as both acmes terminate near the FAD of *M. staurophora*. If the “closed sum problem” (Bralower and Bergen, 1992) were the cause, percent abundances of *M. furcatus* would consistently exceed the 5% threshold across most marl seams. Increased dissolution from burial diagenesis in the marls may have amplified the relative abundance

of *M. furcatus* to some degree, but percent abundances outside the acme range were not close to meeting the requisite 5% threshold throughout all marlstones. The acme begins at 14.9m (Figure 2) and ends at 16.3m, and relative abundances of *M. furcatus* do not exceed 2.5% throughout the remaining section.

Delineating the possible contributing effects of dissolution on assemblage preservation is vital in determining the statistical changes attributable to the enrichment of dissolution resistant. By examining the ratio of etching versus overgrowth and the discrepancies between dissolution resistant and dissolution prone species, we argue that preservation within the limestones was sufficiently good to yield unbiased assemblage data. In contrast, the effect of diagenesis was not sufficiently trivial to warrant any consideration within the marls, despite the fact that %*W. barnesiae* values never exceed the 40% threshold. We partially attribute this coincidental increase in percent abundance as a relic of artificial enrichment. The exact amount of the assemblage attributable to the “closed sum” problem (Burns and Bralower, 1998) is unknown, due to the provincial nature of nannofossils and the lack of well preserved control samples within our study area. The interpretation of preservation intactness is critical, as artificial changes in relative abundances of species can obstruct paleoecological interpretations.

5.3 Nannofossil Paleoecology

Surface water fertility can be accurately interpreted by statistically examining the proportion of nannofossil species adapted to high levels of surface water nutrients. The taxa *Biscutum* spp. and *Zeughrabdotus* spp. are the Mesozoic equivalent of modern small-sized (3-5 μm) calcareous nannoplankton exhibiting opportunistic (r-selected) life strategies in mesotrophic to eutrophic surface water conditions (Watkins, 1989;

Browning and Watkins, 2008). In contrast, assemblages containing relatively higher diversity and equitable distribution of specialist (K-selected) species are interpreted as oligotrophic. Specialist species are more susceptible to ecological displacement by opportunistic species during episodes of nutrient influx (Browning and Watkins, 2008). Relatively low abundances of *Biscutum* spp. (0.9% average) and *Zeugrhabdotus* spp. (7.7% average) suggest that these opportunistic taxa are not crowding out specialists within the assemblage. High Shannon diversity (H) and Evenness (E) indicate ecologically equitable assemblages (Figure 3). Based on these two corroborating criteria, and the lack of correlation of %TOC to any parameter (Table 3), surface water fertility during limestone deposition is interpreted as oligotrophic.

The paucity of these fertility-indicator taxa may also be attributed to oceanographic changes in water circulation that impeded high nutrient surface water conditions. Abundance of *Biscutum* spp. peaked during the Albian/Cenomanian. Brace and Watkins (2014) postulate that the stabilization of ocean circulation, increased surface water stratification, and nutrient partitioning between deep and surface waters may have impeded the conditions necessary to accommodate r-selected life strategies. This paleoecological shift may have been the result of oceanographic changes that lead to widespread chalk deposition during the Late Cretaceous (Brace and Watkins, 2014).

5.3.1 Limestone Nannofossil Paleoecology

The species *D. ignotus* is antithetical to *W. barnesiae* in PCA1 (Figure 3), suggesting that it is the most susceptible to changes in paleoecology and/or preservation conditions within the marls. If this species is prone to dissolution, it is most susceptible relative to all other species observed (Figure 3; Table 3). The moderate imbrication of

calcite elements of *D. ignotus* increases the susceptibility of dissolution when exposed to corrosive pore waters under saturated with respect to calcite. The relatively tighter imbrication of calcite plates of *W. barnesiae*, has lower surface area exposure to corrosive pore water, enabling this taxon to better resist dissolution (Young, et al., 1997). If paleoecology played a predominant role in regulating the relative abundance of *D. ignotus*, lower percent abundances may reflect stressful conditions that inhibit this species to remain at levels comparable to those within the limestones. This suggests that *D. ignotus* may be a specialist (K-selected) species, which is well suited to stable oligotrophic surface water conditions.

5.3.2 Marl Nannofossil Paleoecology

Results from PCA2 indicate that *M. furcatus* played an important role in marlstone paleoecology. The rhythmicity of the interbedded marls and limestones suggest a causal relationship between changes in surface water conditions and Milankovitch cyclicity. However, the poor preservation of nannofossil assemblages within the marls and the lack of contemporaneous species that resemble similar life strategies prevented delineation of a causal relationship. Widespread destruction of Cretaceous marine sediments caused by a shallow carbonate compensation depth (CCD) and the subduction of Pacific continental shelf deposits has further impeded biostratigraphic understanding of the *M. furcatus* acme outside of shallow water epicontinental environments of the WIB and Tethys ocean.

Findings from the Bohemian Cretaceous Basin and the Outer Carpathian of the Czech Republic (Švábenník, and Bubík, 2014) suggest that *M. furcatus* may have had a provincial affinity to surface water conditions similar to that of northern Tethys. The

earliest occurrence of *M. furcatus* was in the Silesian Basin, further south relative to the Bohemian Basin. This cool surface water affinity of *M. furcatus* throughout northern Tethys sediments suggests that northern surface waters expanded south during the Turonian into the Silesian Basin. The diachronous occurrence of *M. furcatus* between Tethys basins serves the basis of this correlation (Švábénick, and Bubík , 2014); however, the authors emphasize the lack of a causal relationship. If strong evidence were to associate *M. furcatus* with relatively cool waters to the north throughout both the WIB and Tethys Sea, higher abundances or unusual diachronous occurrences may indicate changes in surface water conditions.

6.0 Conclusion

A decimeter scale analysis of calcareous nannofossil assemblages from the Fort Hays Member yields geochemical, paleoecological, biostratigraphic data indicating stark differences in preservation between marl and limestone beds in the Fort Hays Member. Preservation was better in the limestone beds, as evidenced by the lack of etched specimens and relatively low percent abundances of *W. barnesiae*. High values of both evenness (E) and Shannon diversity (H), suggests that surface water conditions were oligotrophic during limestone deposition. An interpretation of surface water fertility was impeded within the marls due to the inability to delineate between changes in paleoecology versus the artificial enrichment of dissolution resistant species. Laferriere (1992) suggested that pressure solution during burial remobilized isotopically light carbonate from marls into the adjacent limestones. This proposed mechanism may explain the negative $\delta^{18}\text{O}$ excursions and decrease in nannofossil preservation observed in the marl throughout our study material.

The influence of burial diagenesis increased from west to east across the WIB, in accordance to burial depth (Laferrriere, 1992). Sections in western Kansas were subjected to relatively shallow burial, yet the oscillations between lithologies were still as prevalent as sections to the east. While pressure solution may explain changes in preservation and geochemistry, it alone is insufficient to have driven the differentiation of nanofossils in marls and limestones from a single lithologic precursor. Alternate depositional models argue that clastic influx had a greater influence.

Two sedimentary depositional models have been proposed to explain orbital forced upper Cretaceous chalk. The dilution model claims that lithology was dependent on fluctuations in the clastic influx from the Sevier Highlands, and assumes that biogenic carbonate production was constant. Increased continental runoff would have diluted the carbonates to result in the deposition of calcareous shale/marl. During dry periods, carbonate production would have outpaced clastic influx, resulting in limestone deposition. A millimeter-scale analysis of clays across the Smoky Hill Member and Pierre Shale transition concluded that the rate of clastic deposition remained constant across the boundary (Boesiger, 2005). These findings are consistent with the productivity model, which argues that clastic influx remained relatively constant and that lithology was dependent on the rate of biogenic carbonate production. Appeals to the productivity model lead to the conclusion that if limestones were deposited during oligotrophic surface water conditions, then elevated surface water fertility levels were present during marl deposition; however, the skewing of nanofossil assemblage data attributed to preferential nanofossil dissolution, impedes this assumption. Brace and Watkins (2014) argued that paleoceanographic changes throughout the Late Cretaceous, may have lead to

nutrient partitioning in the water column to establish a stable, oligotrophic, open marine setting. Thus, surface water fertility levels may have remained oligotrophic throughout deposition of both limestones and marls of the Fort Hays Member.

Although paleoecological data within the marls is skewed due to dissolution, *M. furcatus* levels are sufficiently elevated to not have been solely attributable as an artifact of artificial enrichment. The exclusive occurrence of the acme within marls and the close relationship between this species and cool surface water, suggests that changes in cool water circulation may play a role in the acme. A causal relationship cannot be made due to the lack of a contemporaneous equivalent for comparison.

Figures



Figure 1. Map of the Western Interior Seaway during the middle Coniacian (from Blakey, 2015). Locality 1 (star) indicates the location of the Fort Hays Member section examined in this study. The section from Pueblo, Colorado, used for stratigraphic correlations of isochronous bentonite seams and limestone/shale couplets across the basin.

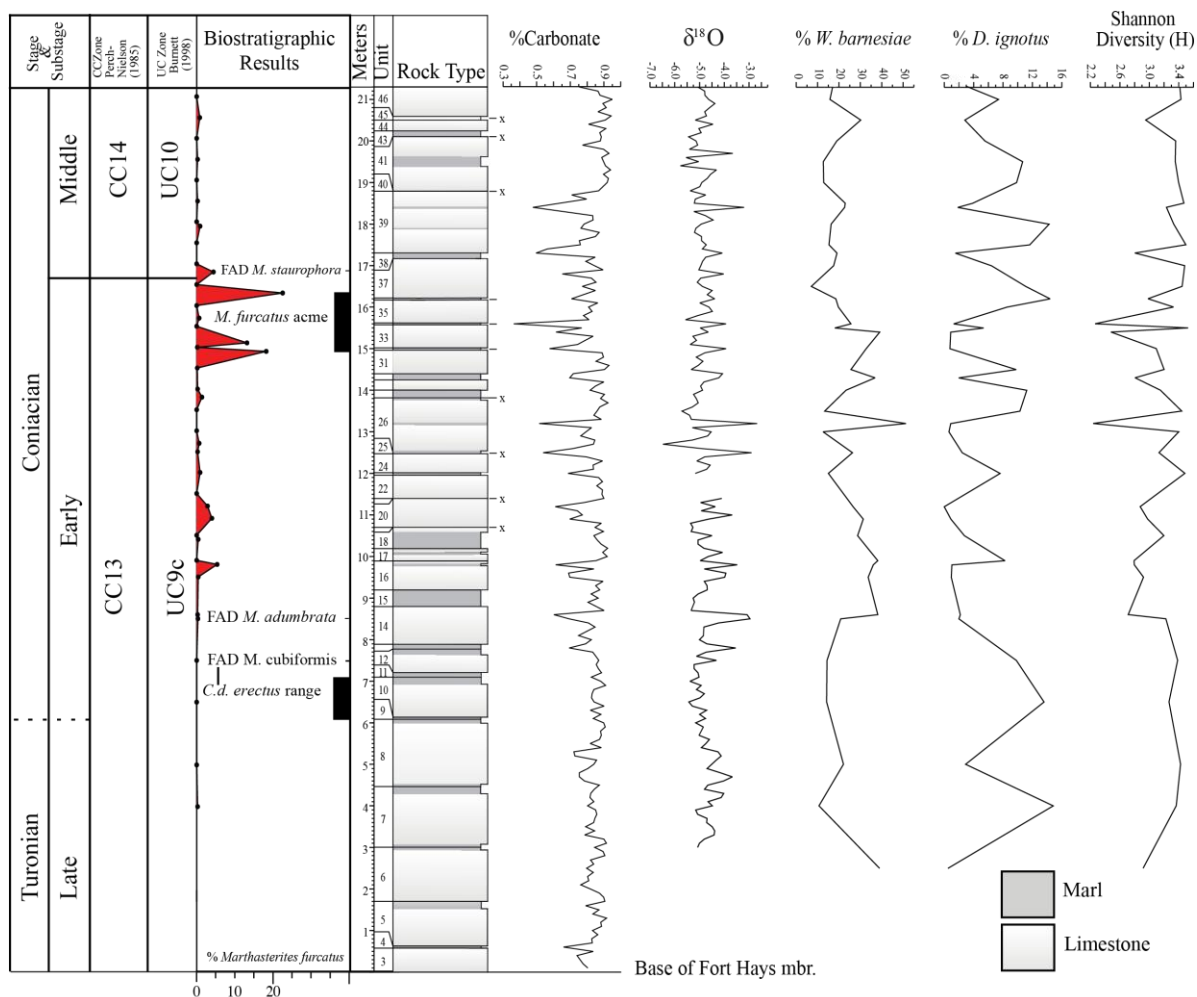


Figure 2. To the right of the stratigraphic column for the Fort Hays Member is the summary of percent total carbonate, average percent *W. barnesiae*, average percent *D. ignotus*, Shannon Diversity, $\delta^{18}O$ isotopic values, and carbon isotope values plotted against Fort Hays Member stratigraphic log and unit markers from Locality 1 (Figure 1), modified from Hattin (1982). To the left of the stratigraphic column is the biostratigraphic zonal scheme for the Fort Hays limestone. Nannofossil bioevents are interpreted using CC (Perch-Nielson, 1985) and (Burnett, 1998) UC zonation schemes. The FAD of *M. cubiformis* occurs at 8.5m, *M. adumbrata* at 8.5m and *M. staurophora* at 16.8m. The FO of *C.d. erectus* is inferred from results correlated from the coeval Fort Hays section at Pueblo, Colorado. Turonian- Coniacian boundary is approximated based on the inferred FAD of *C.d. erectus* (6.1-7.2 m), annotated by a shaded line. The acme of *M. furcatus* is defined by assemblage abundances exceeding 5% and occurs from 9.8-16.3 m.

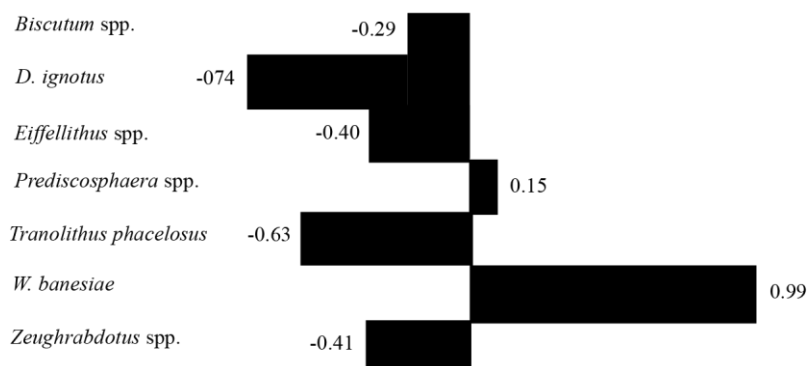


Figure 3. Principle component analysis (PCA1) depicting the variance associated with each species >3% of total assemblage within the Fort Hays member. Negative and positive values are arbitrary and serve to depict the statistical significance of antithetical relationships between taxa. See table 2 for the taxonomy of species listed under the spp. aggregate.

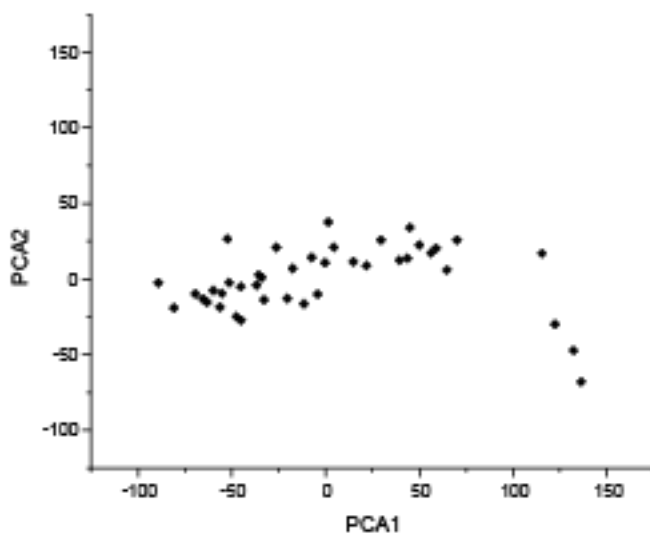


Figure 4. Plot of PCA1 and PCA2 depicting the orthogonal relationship between % *W. barnesiae* and *M. furcatus*. The negatively sloping cluster of four points representing the four *M. furcatus* sample depths (14.9 m, 15.1 m, and 16.3 m) the positively sloping cluster consists of the remaining 36 points representing *W. barnesiae*.

	Etching		Overgrowth
E-1	Slightly jagged outlines of more delicate forms, delicate central area structures damaged in some but not in all specimens.	O-1	Slight overgrowths on central area structures and shield elements.
E-2	More jagged outlines; delicate central structures frequently affected, more delicate forms slightly fragmented.	O-2	Increased overgrowth: some of the more delicate forms become sufficiently masked by secondary calcite to make identification difficult.
E-3	Only the more robust forms are preserved.	O-3	Only the most robust forms are preserved. Reduced diversity due to removal of delicate forms.
E-4	Only fragments of coccoliths preserved; impossible to identify.	O-4	Complete recrystallization; coccoliths no longer identifiable to genus.

Table 1. Qualitative description of etching and overgrowth classifications from Roth (1978).

<i>Biscutum</i> spp.	<i>Biscutum anthracenum</i> <i>Biscutum constans</i> <i>Biscutum ubiquen</i> <i>Biscutum zulloi</i>
<i>Eiffelithus</i> spp.	<i>Eiffelithus eximius</i> <i>Eiffelithus gorkae</i> <i>Eiffelithus turriseifelli</i> <i>Eiffelithus</i> sp.
<i>Prediscosphaera</i> spp.	<i>Prediscosphaera cretacea</i> <i>Prediscosphaera spinosa</i> <i>Prediscosphaera</i> sp.
<i>Zeughrabdotus</i> spp.	<i>Zeughrabdotus elegans</i> <i>Zeughrabdotus erectus</i> <i>Zeughrabdotus noliae</i> <i>Zeughrabdotus</i> sp.

Table 2. Nannofossil taxonomy consists of species that were aggregated together based on similar paleoecological niches and/or taxonomic classification. These taxa constitute >3% of the assemblage for principle component analysis 1 (PCA1).

	CaCO ₃	<i>W. barnesiae</i>	<i>D. ignotus</i>	Shannon	Eveness	Richness	%TOC	$\delta^{13}\text{C}_{\text{org}}$
CaCO ₃		<i>-0.57</i>	<i>0.43</i>	<i>0.59</i>	<i>0.54</i>	<i>0.50</i>	0.13	-0.05
<i>W. barnesiae</i>	<i>-0.52</i>		<i>-0.87</i>	<i>-0.87</i>	<i>-0.86</i>	<i>-0.64</i>	-0.14	0.03
<i>D. ignotus</i>	<i>0.43</i>	<i>-0.87</i>		<i>0.50</i>	<i>0.57</i>	<i>0.29</i>	0.12	-0.04
$\delta^{18}\text{O}$	<i>-0.58</i>	<i>0.41</i>	<i>-0.44</i>	<i>-0.47</i>	<i>-0.46</i>	<i>-0.39</i>	-0.06	0.08
$\delta^{13}\text{C}_{\text{carb}}$	<i>-0.51</i>	<i>0.39</i>	<i>-0.58</i>	<i>-0.41</i>	<i>-0.46</i>	-0.23	-0.25	0.25
$\delta^{13}\text{C}_{\text{org}}$	-0.05	0.03	-0.04	0.01	-0.01	0.02	0.02	
%TOC	-0.13	-0.14	0.13	0.05	0.06	0.07		0.01

Italic type is significant at 95% confidence interval
 Bold type is significant at 99% confidence interval
 Values are Pearson coefficients

Table 3. Pearson correlation coefficients for Figure 2. R-values involving $\delta^{18}\text{O}$, %TOC, carbonate (CaCO₃), $\delta^{13}\text{C}_{\text{carb}}$, and $\delta^{13}\text{C}_{\text{org}}$ have n values of 191. R-values involving *W. barnesiae*, *D. ignotus*, Shannon diversity, evenness, and richness have n values of 41.

	Species Richness (S)			Shannon Diversity (H)			Eveness (E)		
	Min	Max	Avg.	Min	Max	Avg.	Min	Max	Avg.
Marl	37	73	57	1.98	3.48	2.81	0.20	0.51	0.31
Limestone	47	77	68	2.79	3.53	3.29	0.31	0.48	0.40

Table 4. Paleocological results from the Fort Hays Member presented in minimums, maximums, and averages.

	%TOC			$\delta^{13}\text{C}_{\text{carb}}$			$\delta^{13}\text{C}_{\text{org}}$			$\delta^{18}\text{O}$		
	Min	Max	Avg.	Min	Max	Avg.	Min	Max	Avg.	Min	Max	Avg.
Marl	0.41	4.99	1.27	0.74	2.02	1.58	-27.11	-24.21	-26.33	-2.68	-5.38	-4.02
Limestone	0.57	4.80	1.62	0.35	2.23	1.20	-28.48	-17.31	-25.80	-3.66	-6.47	-4.90

Table 5. Geochemical results from the Fort Hays Member presented in minima, maxima, and averages.

	CaCO ₃	<i>W. barnesiae</i>	<i>D. ignotus</i>	Shannon	Eveness	Richness	Limestone AVG	Marl AVG	% Change
<i>E. floralis</i>	-0.79	0.51	-0.51	-0.63	-0.56	-0.56	0.41%	1.13%	+175.61%
<i>L. septanarius</i>	-0.59	0.55	-0.55	-0.71	-0.71	-0.58	1.11%	2.99%	+169.37%
<i>M. furcatus</i>	-0.43	0.06	-0.06	-0.63	-0.57	-0.55	0.24%	4.94%	+1958.33%
<i>P. cretacea</i>	0.17	0.19	-0.25	-0.14	-0.15	-0.21	6.89%	8.06%	+16.98%
<i>Prediscosphaera spp.</i>	-0.06	0.13	-0.26	-0.04	-0.04	-0.14	10.02%	10.97%	+9.48%
<i>Q. gartneri</i>	-0.38	0.48	-0.46	-0.47	-0.42	-0.41	0.56%	1.18%	+110.71%
<i>W. barnesiae</i>	-0.57		-0.87	-0.87	-0.88	-0.64	19.77%	33.13%	+67.58%
<i>Z. embergeri</i>	-0.06	0.01	-0.14	-0.16	-0.27	-0.18	1.59%	1.73%	+8.81%

Italic type is significant at 95% confidence interval
 Bold type is significant at 99% confidence interval
 Values are Pearson coefficients

Table 6. Pearson correlation coefficients of dissolution resistant species measured against: percent carbonate (CaCO₃), average percent abundance of *W. barnesiae*, average percent abundance of *D. ignotus*, paleoecological parameters, average abundance dissolution resistant species within limestones and marls, and the percent difference between lithologies. R-values are calculated using n=41.

	CaCO ₃	<i>W. barnesiae</i>	<i>D. ignotus</i>	Shannon	Eveness	Richness	Limestone AVG	Marl AVG	% Change
<i>Biscutum spp.</i>	0.20	-0.40	0.59	0.50	0.54	0.49	1.01%	0.52%	-49.10%
<i>C. garrisonii</i>	0.34	-0.22	0.13	0.35	0.22	0.39	1.22%	0.81%	-33.61%
<i>C. ehrenbergii</i>	0.06	-0.32	0.38	0.16	0.27	0.41	1.73%	1.58%	-8.67%
<i>D. ignotus</i>	0.43	-0.87		0.50	0.57	0.29	7.05%	2.89%	-59.00%
<i>Eiffellithus spp.</i>	0.23	-0.45	0.06	0.49	0.45	0.41	5.38%	4.45%	-17.28%
<i>L. carniolensis</i>	0.28	-0.36	0.40	0.40	0.48	0.17	0.61%	0.37%	-39.34%
<i>T. phacelosus</i>	0.54	-0.14	0.57	0.68	0.68	0.61	10.12%	6.64%	-34.38%
<i>Zeughrabdotid spp.</i>	-0.28	-0.49	0.12	0.52	0.58	0.26	8.32%	6.33%	-23.91%

Italic type is significant at 95% confidence interval
 Bold type is significant at 99% confidence interval
 Values are Pearson coefficients

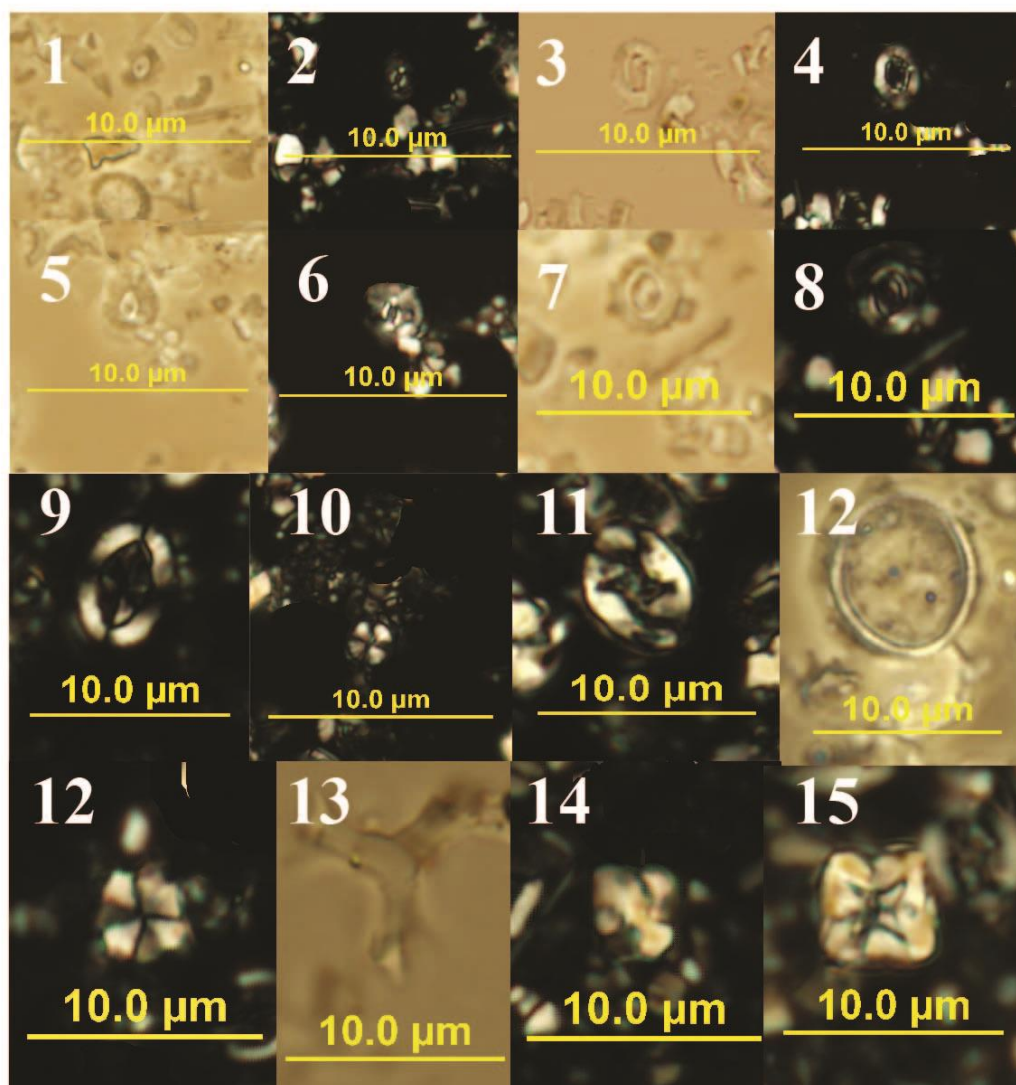
Table 7. Pearson correlation coefficients of dissolution prone species measured against: percent carbonate (CaCO₃), average percent abundance of *W. barnesiae*, average percent abundance of *D. ignotus*, paleoecological parameters, average abundance of dissolution prone species within limestones and marls, and the percent difference between lithologies. R-values are calculated using n=41.

References

- Blakey, R.C. 2015, North American Paleogeographic Maps. Colorado Plateau Geosystems.
- Boesiger, T.M. 2005, Response of calcareous nannofossil assemblages to regression of the Niobrara Sea. (M.S. Thesis) University of Nebraska-Lincoln.
- Bowman, A.R. and Bralower, T.J., 2005, Paleoceanographic significance of high-resolution carbon isotope records across the Cenomanian–Turonian boundary in the Western Interior and New Jersey coastal plain, USA: *Marine Geology*, v. 217, p. 305–321.
- Brace, B., and Watkins, D.K., 2014, Evolution of the calcareous nannofossil genus *Biscutum* in the middle to Upper Cretaceous North American mid-latitudes: *Micropaleontology*, v. 60, p. 445-463.
- Bralower, T.J. and Bergen, J.A., 1998, Cenomanian-Santonian Calcareous Nannofossil Biostratigraphy Of A Transect Of Cores Drilled Across The Western Interior Seaway: Stratigraphy and Paleoenvironments of the Cretaceous Western Interior Seaway, USA, p. 59–77.
- Browning, E.L. and Watkins, D.K., 2008, Elevated primary productivity of calcareous nanoplankton associated with ocean anoxic event 1b during the Aptian/Albian transition (Early Cretaceous): *Paleoceanography*, v. 23.
- Burnett, J. 1998, Upper Cretaceous, in Bown, P.R. (Ed.), *Calcareous Nannofossil Biostratigraphy*: Chapman and Hall, Cambridge, p. 132-199.
- Burns, C.E. and Bralower, T.J., 1998, Upper Cretaceous Nannofossil Assemblages Across The Western Interior Seaway: Implications For The Origins Of Lithologic Cycles In The Greenhorn And Niobrara Formations: Stratigraphy and Paleoenvironments of the Cretaceous Western Interior Seaway, USA, p. 35–58.
- Chang, Y.-M. 1967, Accuracy of fossil percentage estimation: *Journal of Paleontology*, v. 41, p. 500-502.
- Corbett, M. Watkins, D., and Pospichal, J., 2014, A quantitative analysis of calcareous nannofossil bioevents of the Late Cretaceous (Late Cenomanian–Coniacian) Western Interior Seaway and their reliability in established zonation schemes: *Marine Micropaleontology*, v. 109, p. 30–45.
- Eicher, D.L., and Diner, R., 1985, Foraminifera as Indicators of Water Mass in the Cretaceous Greenhorn Sea, Western Interior: Fine-Grained Deposits and Biofacies of the Cretaceous Western Interior Seaway, p. 60–71.
- Frank, T.D., Arthur, M.A. and Dean, W.E., 1999, Diagenesis of lower cretaceous pelagic carbonates, north Atlantic: Paleoceanographic signals obscured: *Journal of Foraminiferal Research*, v. 29, no. 4, p. 340-351.
- Gilbert, G.K. 1895, Sedimentary measurement of Geologic time: *Journal of Geology*, v.3 p. 121-127.
- Hammer, Ø. Harper, D.A.T., Ryan, P.D., 2001, PAST: Paleontological statistics software

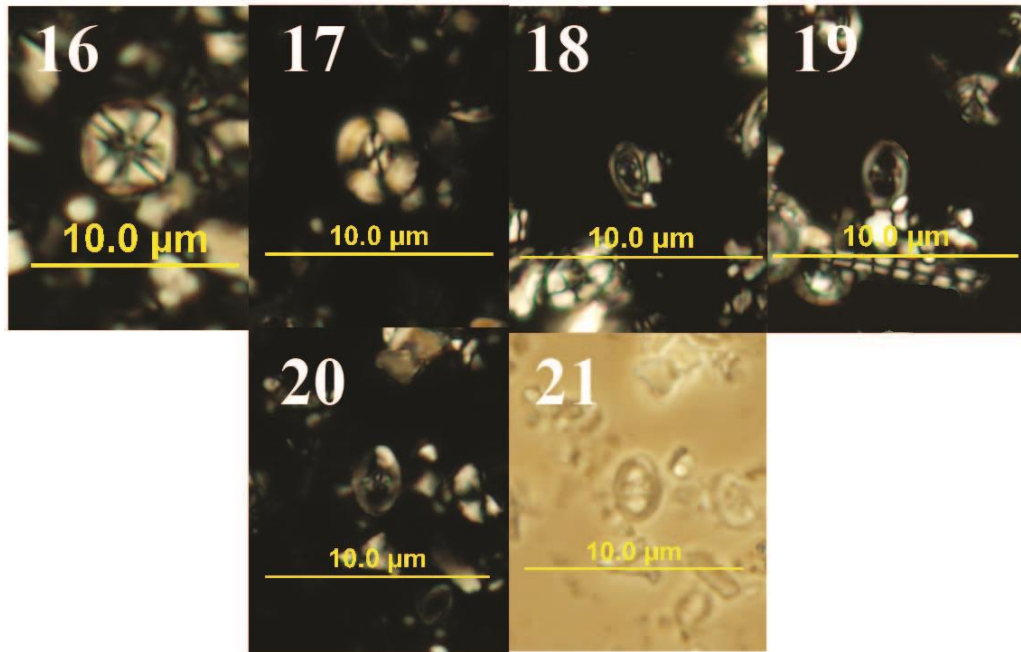
- package for education and data analysis: *Palaeontologia Electronica*, v. 4, p. 9.
- Hattin, D.E. 1975, Stratigraphic study of the Carlile-Niobrara (Upper Cretaceous) unconformity in Kansas and northeastern Nebraska, Geological Association of Canada, Special Publication 13, 195-210.
- Hattin, D.E. 1982, Stratigraphy and depositional environment of Smoky Hill Chalk Member, Niobrara Chalk (Upper Cretaceous) of the type area, western Kansas: Kansas Geological Survey Bulletin, v. 225, p. 1-108.
- Kauffman, E.G., 1977, Geological and biological overview: Western Interior Cretaceous Basin: *The Mountain Geologist*, v. 14, p. 75-99.
- Kauffman, E.G., Caldwell, W.G.E., 1993, The Western Interior Basin in space and time. In: Caldwell, W.E., Kauffman, E.G. (Eds.), *Evolution of the Western Interior Basin*. Special Papers Geological Association of Canada, v. 39, p. 1-30.
- Kita, Z.A., Watkins, D.K., 2014, *Calcareous Nannofossils From The Niobrara Formation (Late Cretaceous) Western Interior Seaway, USA: Unpublished Ph.D. dissertation, University of Nebraska-Lincoln, Nebraska, 88 pp.*
- Laferriere, A.P., 1992, Regional isotopic variations in the Fort Hays Member of the Niobrara Formation, United States Western Interior: Primary signals and diagenetic overprinting in a Cretaceous pelagic rhythmite: *Geological Society of America Bulletin*, v. 104, p. 980-992.
- Logan, W.N., 1897, The Upper Cretaceous of Kansas. Kansas University Geological Survey 2, p. 195-234.
- Meek, F.B., Hayden, F.V., 1861, Descriptions of new Silurian (Primordial), Jurassic, Cretaceous, and Tertiary fossils collected in Nebraska by the exploring expedition under the command of Capt. William F. Reynolds, U.S. Topographical Engineers, with some remarks on the rocks from which they were obtained: *Proceedings, Academy of Natural Sciences of Philadelphia*, v. 13, p. 415-447.
- Perch-Nielsen, K. 1985, *Mesozoic calcareous nannofossils: Plankton Stratigraphy*, Cambridge University Press, Cambridge, p. 329-426.
- Pielou, E. C., 1969, *An Introduction to Mathematical Ecology*: John Wiley, New York, 286 pp.
- Pratt, L.M., 1981, A paleo-scenographic interpretation of the sedimentary structures, clay minerals, and organic matter in a core of the Middle Cretaceous Greenhorn Formation near Pueblo, Colorado: Princeton, N.J., Princeton University, Ph.D. Thesis, 176 pp.
- Riesselman, C.R., 2000, Carbonate content cycles from the Santonian-Campanian boundary, Niobrara Formation, western Kansas: Unpublished undergraduate thesis, University of Nebraska-Lincoln, Nebraska, 20 pp.
- Roth, P.H., 1978, Cretaceous nannoplankton biostratigraphy and oceanography of the northwestern Atlantic Ocean: *Initial Reports of the Deep Sea Drilling Project*, v. 44, p. 731-759.

- Roth, P.H. and Bowdler, J.L., 1981, Middle Cretaceous Calcareous Nannoplankton Biogeography And Oceanography Of The Atlantic Ocean: The Deep Sea Drilling Project: A Decade of Progress, p. 517–546.
- Sageman, B.B., Singer, B.S., Meyers, S.R., Siewert, S.E., Walaszczyk, I., Condon, D.J., Jicha, B.R., Obradovich, J.D., and Sawyer, D.A., 2014, Integrating $^{40}\text{Ar}/^{39}\text{Ar}$, U-Pb, and astronomical clocks in the Cretaceous Niobrara Formation, Western Interior Basin, USA: Geological Society of America Bulletin, v. 126, p. 956–973.
- Scott, G.R., Cobban, W.A., 1964. Stratigraphy of the Niobrara Formation at Pueblo, Colorado: U.S. Geological Survey Professional Paper, Report 0454-L, L1-L30.
- Švábenická, L. and Bubík, M., 2014, Biostratigraphical correlations of the calcareous nannofossil *Marthasterites furcatus* in the Bohemian Cretaceous Basin and Outer Flysch Carpathians, Czech Republic: Cretaceous Research, v. 51, p. 386–398.
- Watkins, D.K., 1986. Calcareous nannofossil paleoceanography of the Cretaceous Greenhorn Sea. Geological Society of America Bulletin 97, 1239-1249.
- Watkins, D.K., 1989. Nannoplankton productivity fluctuations and rhythmically-bedded pelagic carbonates of the Greenhorn Limestone (Upper Cretaceous). Palaeogeography, Palaeoclimatology, Palaeoecology, v. 74, p. 75-86.
- Watkins, D.K., and Bergen, J.A., 2003, Late Albian adaptive radiation in the calcareous nannofossil genus *Eiffellithus*: Micropaleontology, v. 49, 231 pp.
- Watkins, D.K., M.J. Cooper, and P.A. Wilson, 2005, Calcareous Nannoplankton Response to late Albian Oceanic Anoxic Event 1d in the Western North Atlantic, Paleoceanography, v. 20, 14 pp.
- Williams, J.R., and Bralower, T.J., 1995, Nannofossil assemblages, fine fraction stable isotopes, and the paleoceanography of the Valanginian-Barremian (Early Cretaceous) North Sea Basin: Paleoceanography, v. 10, p. 815–839.
- Young, J.R., Bergen, J.A., Burnett, J.A., Fiorentino, A., Jordan, R.W., Kleijne, A., Von Niel, B.E., Romein, A.J.T., and Von Salis, K., 1997, Guidelines for coccolith and calcareous nannofossil terminology: The Palaeontological Association, v. 40, p. 875–912.



XPL Cross Polarized Light, PL Plane Light, PC Phase Contrast

1. *Biscutum anthracenum* Brace and Watkins (2014), PC. 2. *Biscutum anthracenum*, XPL. 3. *Biscutum constans* Górka (1957), PC. 4. *Biscutum constans*, XPL. 5. *Biscutum ubiquem* Brace and Watkins (2014), PC. 6. *Biscutum ubiquem*, XPL. 7. *Biscutum zulloi* Covington (1994), PC. 8. *Biscutum zulloi*, XPL. 9. *Broinsonia furtiva* Bukry (1969), XPL. 10. *Discorhabdus ignotus* Górka (1957), XPL. 11. *Eiffellithus eximius* Stover (1966), XPL. 12. *Kampnerius magnificus* Deflandre (1959), PC. 13. *Lithastrinus septanarius* Forchheimer (1972), XPL. 14. *Marthasterites furcatus* Deflandre and Fert (1954), PL. 15. *Micula adumbrata* Burnett (1997), XPL. 16. *Micula cubiformis* Forchheimer (1972), XPL.



XPL Cross Polarized Light, PL Plane Light, PC Phase Contrast

16. *Micula decussata* Vekshina (1959), XPL. 17. *Watznaueria barnesiae* (Black, 1959), XPL. 18. *Zeughrabdotus clarus* Deflandre in Deflandre & Fert (1954), XPL. 19. *Zeughrabdotus elegans* Gartner (1968), XPL. 20. *Zeughrabdotus noeliae* Rood et al. (1971), XPL. 21. *Zeughrabdotus noeliae*, PC.